Eaves connections of double-bay portal frames with staggered single channel cold-formed rafters

B. Tshuma & M. Dundu
Department of Civil Engineering Science, University of Johannesburg, P O Box 524, Auckland Park 2006, South Africa

ABSTRACT: Experimental tests were performed to evaluate the structural performance of the eaves region of double-bay portal frames with staggered cold-formed rafters. This region represents the distance from the point of maximum moment at the eaves joint to the point of zero moment (contraflexure) in the rafters and columns respectively. The column and two rafter members are formed from single cold-formed channel sections, which are bolted back-to-back at the eaves joint. In order to simplify the connections the rafters are connected directly to the back of the web of the column at different levels. Particular attention was focused on the failure modes of the structures, the strength (resistance to moment) of the connection, the moment-curvature performance and the connection's ability to form plastic hinges. In all the tested structures, the column failed by local buckling in the compression flange and web, between the upper and lower rafters. The moment-curvature graphs proved that plasticity could not be achieved in these connections.

1 INTRODUCTION

Portal frames made from cold-formed steel as the primary frame have been on the increase during the past 20 years. However, the challenge has always been on the efficiency and economy of the connecting systems of the members. The objective of this investigation is to evaluate the structural performance of the eaves connection of a double-bay portal frame with staggered cold-formed rafters. The investigation will also determine whether the portal frame can be designed plastically or not.

The investigation focuses on the eaves connection of double-bay portal frames formed from single cold-formed steel channels. In a double-bay portal frame, the columns of two single-bay portal frames, positioned adjacent to each other, are replaced by one internal column. The majority of double and/or multi-bay portal frames have slender internal columns because the moments at the eaves connection balance each other when the portal frame is subjected to vertical downward loading. This allows the internal column to be designed for compression forces only. However, in this investigation, the two cold-formed rafters are connected, back-to-back, to the column, with one rafter connected to the column at a lower level than the other as shown in Figure 1.

The connection configuration results in the development of an unbalanced moment in the column. Although this moment acts on a short segment of the column, it should be taken into consideration when analyzing and designing the frame. The connection is simply to design, fabricate and construct since it uses 4, M20 bolts per rafter-column joint and less materials, as no secondary member(s) like gusset plates or cleats are used.

The back-to-back connection of rafters and column at the eaves joint counterbalance the eccentricities of the connected channels, thus, resisting lateral-torsional buckling of the channels (Dundu & Kemp 2006a, b). However, the structural arrangement of the connection may not be the best from an aesthetic viewpoint.The experimental structure configurations are based on previous research work, performed by Dundu (2003). The span, spacing and eaves height of the frames were kept constant at 12 m, 4.5 m and 3 m, respectively.

Table 1. Average material properties of the cold-formed steel channels

Channel section	Specimen	f_y	f_u	E
		MPa	MPa	GPa
300 × 75 × 20 × 3	LWC	240.828	321.256	207
	LFC	253.900	331.654	
	LCC	366.885	406.089	
300 × 65 × 20 × 3	LWC	228.666	309.215	206
	LFC	240.330	317.852	
	LCC	322.244	375.391	
300 × 50 × 20 × 3	LWC	255.153	335.048	208
	LFC	330.550	367.675	
	LCC	379.962	402.319	

2 MATERIAL PROPERTIES

2.1 *Properties of cold-formed steel channels*

Thirty-three coupons were tested to determine the material properties of the cold-formed steel channels. These include five longitudinal web coupons (LWC) cut from the web, three longitudinal corner coupons (LCC) cut from the corners joining the web and flange, and three longitudinal flange coupons (LFC) cut from the flange. The number of coupons tested was largely dependent on the depth or width of each segment.

LWC and LFC were tested with the intention of using their average ultimate stress and average yield stress to calculate the bearing resistance and moment of resistance of the channels, respectively. This is because webs and flanges largely resist bearing forces and bending moments in connections, respectively. LCC were tested in order to determine the effect of cold rolling at the corners to the yield stress, ultimate stress and ductility, and to ensure and prove that LFC do not inherit the properties of LCC, especially on channels with narrow flanges. Guidelines provided by ISO 6892-1 (2009) were used in the preparation and testing of the cold-formed steel coupons.

The average material properties for the three channel sizes are given in Table 1. LFC of the 300 × 50 × 20 × 3 channel significantly inherited the properties of LCC; hence results of LWC were adopted throughout the investigation, as a conservative approach. Stress-strain graphs for 300 × 75 × 20 × 3 coupons are shown in Figure 2. Similar graphs were plotted to establish the properties of all the tested coupons. The Young's modulus of elasticity (E) of each channel is derived from averaging the slope of the stress-strain curve over the elastic region.

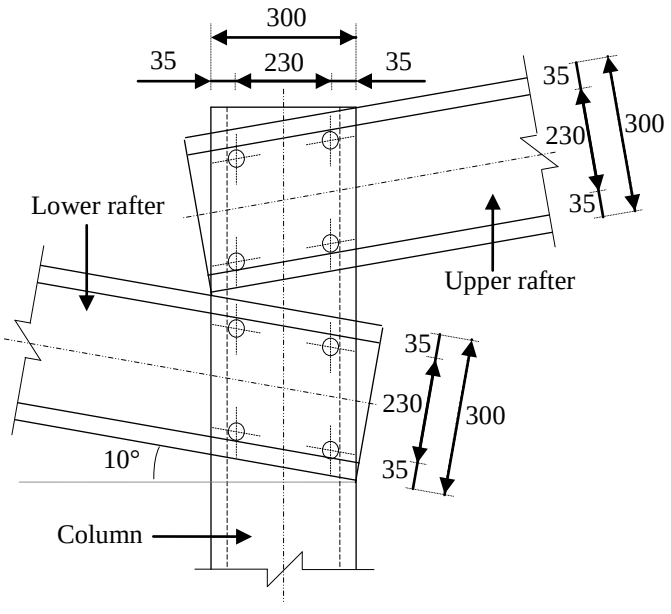

Figure 1. Typical eaves connection structure

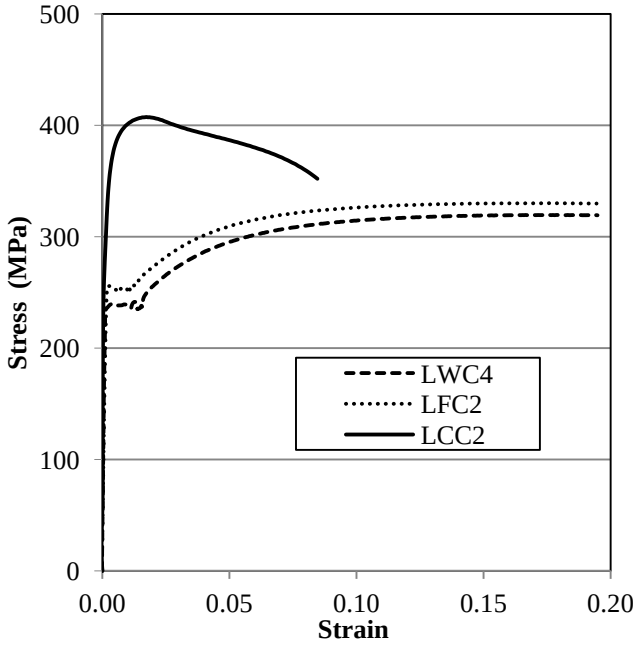

Figure 2. Stress-strain graphs for 300 × 75 × 20 × 3 coupons

2.2 *Bolt properties*

M20, grade 8.8 high strength structural steel bolts were selected for the connections. A shear strength calculation showed that the selected bolts are adequate for all the connections. Material tests on the bolts were not done since the strength of the bolts ($f_u \geq 800$ MPa) is less critical than the bearing strength of cold-formed steel channels used. A 2 mm bolt-hole clearance was adopted to reduce large slips in the connections and standard steel washers were placed on both sides of the bolt to prevent excessive rotation of the bolt.

3 EXPERIMENTAL INVESTIGATION

3.1 *Representative model of the test structures*

An experimental model was developed to represent, as much as possible, the behaviour of a double-bay portal frame structure. The model was developed to simulate the boundary conditions of a full double-bay portal frame structure. Testing of a full double-bay portal frame structure was avoided because of the cost and the limited space in the laboratory. The test model was taken from the central eaves joint (point D) to the points of contraflexure in the rafters (points B and C) and column (point A) as shown in Figure 3. Material properties (yield stress (f_y), ultimate strength (f_u) and Young's modulus of elasticity (E)) and the width of the channel flanges were the experiment variables. The depth and thickness of the channels were not varied. Three different frames (Structures 1, 2 and 3) were tested to evaluate the effect of the flange width and material properties to the structural performance of the central eaves joint.

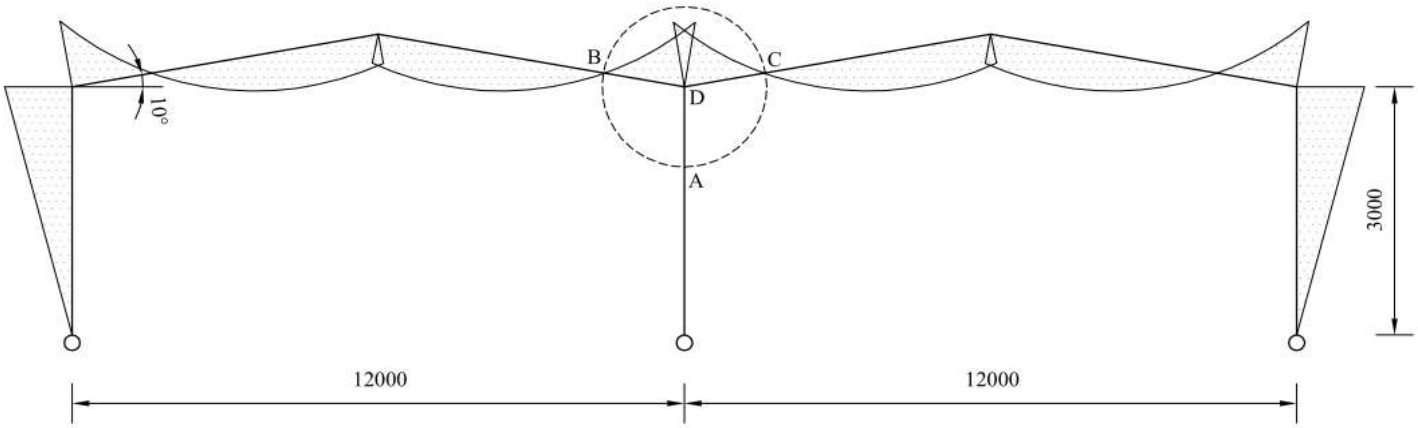

Figure 3. Typical bending moment diagram of the complete double-bay portal frame subjected to vertical downward loading.

3.2 *Test configuration and instrumentation*

The layout and geometry of the test set-up is shown in Figure 4. Points A and D are the load application points in the lower rafter (LR) and upper rafter (UR), respectively, while points E and F are the load application points in the in the column. Points B and C represents the lower rafter-to-column and upper rafter-to-column joints, respectively. Point G is the base of the column. The lever arm (*e*) is the perpendicular distance from the upper rafter-to-column and lower rafter-to-column connections to the applied load (P).

Electronic clinometers were mounted vertically at the centre of each joint inside both rafters to measure the rotation of the joints. Strains, just outside the joint, were measured using strain gauges. A data-logging equipment was used to collect data from the rotations and strains. The load was applied using two, 10 ton jacks, and calibrated against time through the load display software.

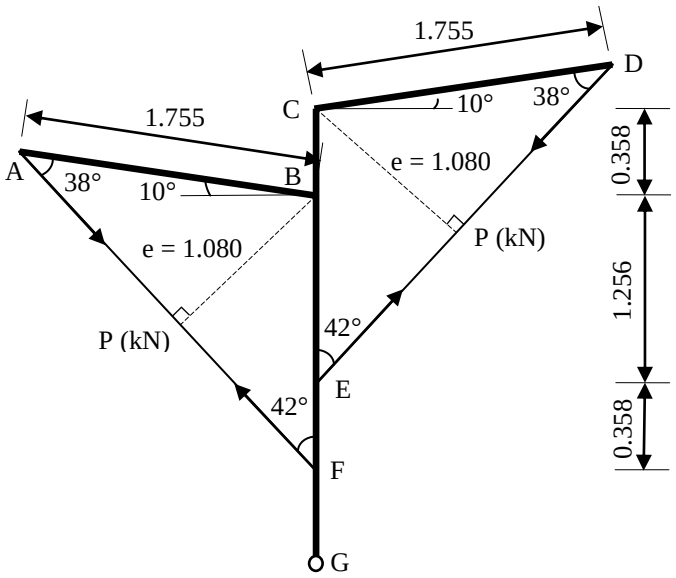

Figure 4. Layout and geometry of the test set-up

3.3 *Experimental procedure*

The test structures were assembled on the laboratory floor and lifted into the testing platform using a crane. The two rafters were subjected to simultaneous equal loads applied through flat bars at the points of contraflexure. To prevent twisting, the load was applied through the shear centre. Horizontal movement of the structure was controlled by the restraints through Alwayse ball transfer units. Alwayse ball transfer units also facilitated a frictionless movement of the rafters, in-between the rafter restraints.

Load increments of 0.5 kN at two minutes intervals were applied up to ninety percent of the anticipated failure load. Thereafter, the loading interval was increased to three minutes. This was done so as to visually monitor the final critical stages that the structure undergoes before failing.

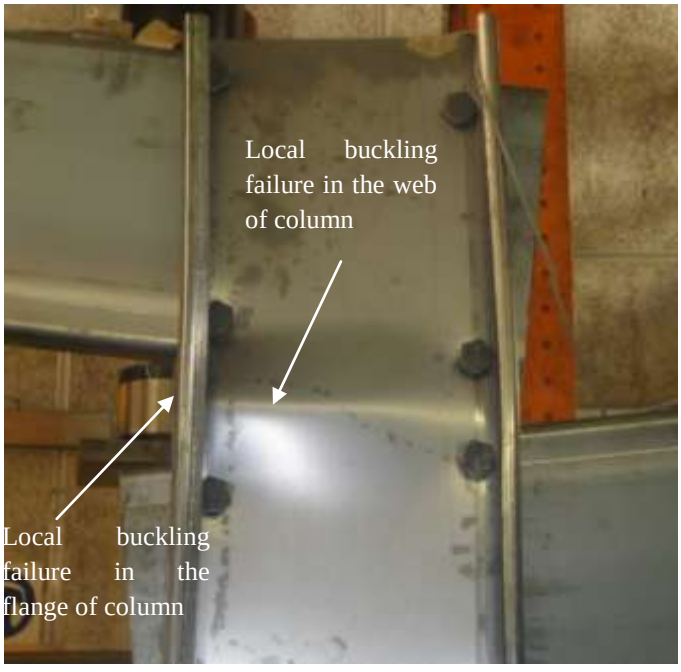

Figure 5. Local buckling failure

4 FAILURE MODES

Local buckling and bolt-bearing deformations were the observed failure modes in all the structures. In all the tested structures, local buckling of the compression flange and web of the column was the eventual failure mechanism. Local buckling started on the compression web of the column and extended horizontally along the web of the column as shown in Figure 5. This failure is attributed to the unbalanced moment in the column caused by connecting rafters at different levels, as shown in Figure 6.

After testing, bolt-hole elongations were measured and found to range from 1.5 mm to 2.5 mm. All bolt-holes elongated in the direction of the bolt force due to moments. This proves that the bolt forces due to moments contribute more to the resultant bolt forces, compared to bolt forces due to axial and shear forces. Although significant bolt-hole distortions were observed in all connections after disassembling the frames, the connections did not fail as a result of the bearing distortions.

5 CAPACITY OF CHANNELS AND JOINTS

The yield moment (M_y), axial load (N_y) and shear resistance (V_r) are calculated, based on the effective cross-sectional properties of the cold-formed channels, to allow for local buckling, as given in Equations 1, 2 and 3.

$$M_y = Z_{ef} f_y \quad (1)$$

$$N_y = A_{ef} f_y \quad (2)$$

$$V_r = A_w f_v \quad (3)$$

where Z_{ef} = effective section modulus; f_y = yield stress of the channel section; A_{ef} = effective cross-sectional area of the channel section; A_w = effective cross sectional area of the web; and f_v = limiting shear stress.

All the tested structures failed to achieve the theoretical elastic resistances of the cold-formed steel channels. The failure to achieve the theoretical resistances of the channels was caused by local buckling failure of the column which took place before the joints failed.

In all the tested frames, the yield moment (M_y) of the channels is greater than the maximum moment (M_{ux}) (Table 4). This means that the column did not fail by yielding. The ratios of M_{ux} to M_y for Structures 1, 2 and 3 are 0.77, 0.83 and 0.94, respectively. The higher ratio of Structure 3 can be attributed to the high yield strength of the 300 × 50 × 20 × 3 channel, compared to other channels.

The theoretical moment of resistance of the joint (M_{rj}) is computed from the bearing resistance of the thickness of the connected members, because the bearing resistance (B_r) of the plate is more critical than the shearing resistance of the bolts (V_{rb}). Equations 4 and 5 give the bearing resistance (B_r) of the connected member and the unfactored shear resistance of each bolt (V_{rb}), respectively.

$$B_r = atf_u \leq Cdtf_u \quad (4)$$

$$V_{rb} = 0.7 \times 0.60 m A_b f_{ub} \quad (5)$$

where a = distance from the bolt-hole centre to the edge, in the direction of the force; t = minimum thickness of the connected parts; f_u = minimum tensile strength of the channel; C = bearing resistance factor of fasteners (Kemp (2001)); d = nominal diameter of the fastener; A_b = cross-sectional area of fastener based on nominal diameter; and m = number of faying surfaces or shear planes in a bolted joint; f_{ub} = is the tensile strength of the bolt.

The theoretical moment of resistance of the joint (M_{rj}) is calculated from the bearing resistance (B_r) and the lever arm (e) of each bolt in the connection. The comparison of maximum moments (M_{ux}) and yield moments (M_y) and the theoretical moment of resistance of joints (M_{rj}) are shown in Table 2.

In all tested structures, M_{rj} is larger than M_{ux}, indicating that the capacity of the joints is not critical. The ratio of maximum moment (M_{ux}), to the theoretical moment of resistance of joints (M_{rj}) for Structures 1, 2 and 3 is 0.95, 0.94 and 0.95 respectively. This is an indication that the joints did not fail since their capacity was not attained.

Generally, channels with wider flanges resist larger moments than those with smaller flanges, provided that the channels are of the same material properties. Despite having the smallest flange channel (50 mm), Structure 3 exhibited the largest maximum moment (M_{ux}). This is attributed to the high material strength of the 300 × 50 × 20 × 3 channel.

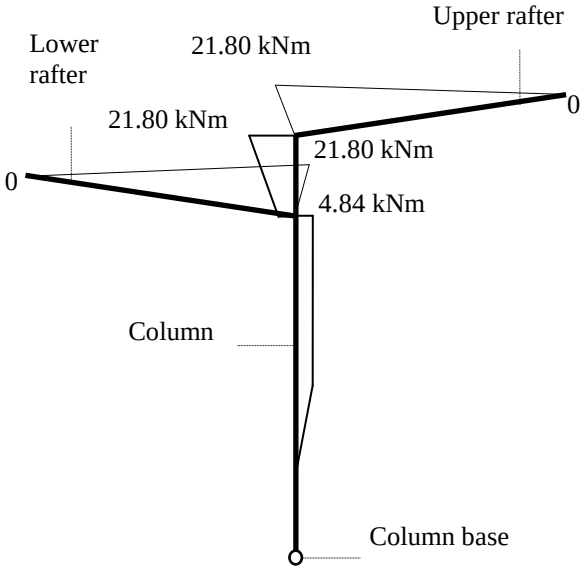

Figure 6. Bending moment diagram of Structure 1

Table 2. Comparison of ultimate and yield moments, and theoretical moment of resistance of joints

Structure No.	Channel size	f_y MPa	f_u MPa	P kN	e m	M_{ux} kNm	M_y kNm	M_{ux}/M_y	B_r kN	M_{rj} kNm	M_{ux}/M_{rj}
1	300 × 75 × 20 × 3	240.828	321.256	20.18	1.08	21.80	28.15	0.77	34.70	22.83	0.95
2	300 × 65 × 20 × 3	228.666	309.215	19.05	1.08	20.57	24.72	0.83	33.40	21.97	0.94
3	300 × 50 × 20 × 3	255.153	335.048	21.02	1.08	22.70	24.09	0.94	36.19	23.81	0.95

Table 3. Average maximum moment, rotation, secant rotational stiffness of the joint and curvature results

Structure No.	Channel size	f_y MPa	M_{ux} kNm	ϕ_{max} Rad.	ϕ_{sj} kNm/rad	K_{max} (1/mm) 10E-6
1	300 × 75 × 20 × 3	240.828	21.80	0.033	660.61	10.41
2	300 × 65 × 20 × 3	228.666	20.57	0.032	642.81	7.16
3	300 × 50 × 20 × 3	255.153	22.70	0.033	687.88	5.28

Structure 3 also exhibited the largest bearing resistance (B_r) and theoretical moment of resistance of the joint (M_{rj}) compared to Structure 1 and 2 since the B_r and the M_{rj} are a function of the high ultimate tensile strength of the 300 × 50 × 20 × 3 channel compared to that of the other channels.

6 MOMENT-ROTATION AND CURVATURE CURVES

The average maximum moments, rotations, curvatures and joint rotational stiffness results for all the tested structures are shown in Table 3. These maximum moments, rotations, curvatures and joint rotational stiffness values are the maximum values at column failure and not at joint failure since the joint did not fail in all the structures. Figure 7 shows the average moment-rotation curves of the upper rafter and lower rafter for all the tested structures.

The average secant rotational stiffnesses of the joint (ϕ_{sj}) at column failure show that Structure 3 produced the highest stiffness of 688 kNm/rad followed by Structure 1 and 2 with stiffnesses of 661 kNm/rad and 643 kNm/rad, respectively. The average moment-curvature curves for all the frames (Figure 8) show a linear range followed by a non-linear range, save for Structure 1 LR and Structure 2 UR whose graphs show a linear range followed by non-linear range with various random slips within the elastic ranges and an initial slip followed by a linear range, respectively. The graphs show that plasticity was not achieved in all the tested frames.

7 CONCLUSION

Local buckling of the web and flange of the column, and bolt-bearing deformations were the observed failure mechanisms.

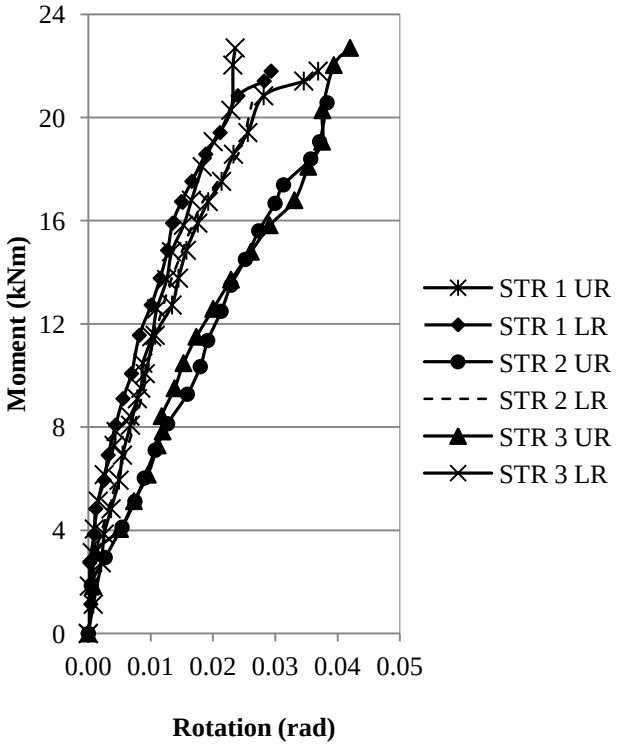

Figure 7. Average moment-rotation curves for all frames

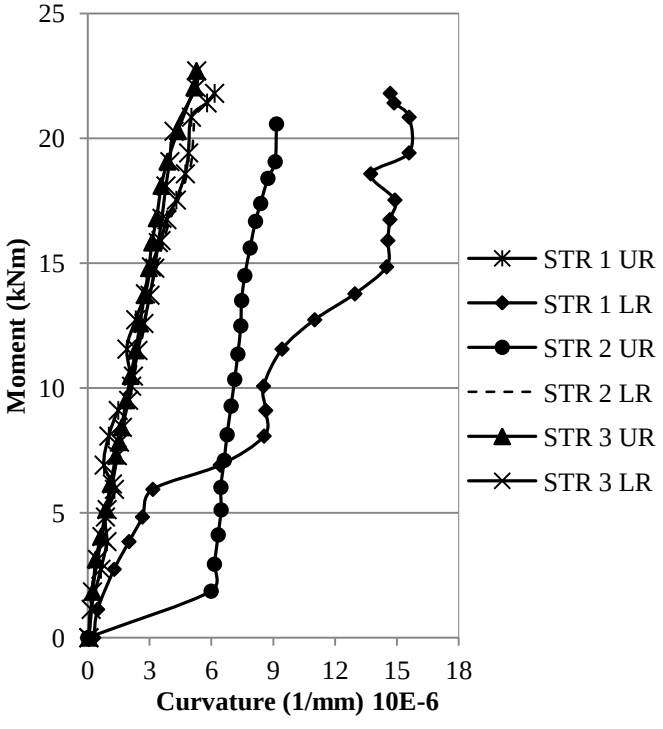

Figure 8. Average moment-curvature curves for all frames

However, local buckling was the ultimate failure mode in all structures. Local buckling was caused by the unbalanced moment in the column.

The material properties of the channels influenced the structures' performance more than the flange widths of the channels. This explains why Structure 3 achieved the largest ultimate moment (M_{ux}) compared to Structure 1 and 2.

To be able to understand and analyse the structural performance and behaviour of the eaves connections of double-bay portal frames with staggered single channel cold-formed rafters, the joints must fail and for that to happen, certain test parameters have to be changed.

REFERENCES

DIN EN 1993-1-1. Design of steel structures: Part 1.1 – General rules and rules for buildings. Brussels: *European Committee of Standardization (CEN)*: 2010-12.

Dundu, M. 2011. Design approach of cold-formed steel portal frames. *International Journal of Steel Structures* 11(3): 259-273.

Dundu, M. & Kemp, AR. 2006a. Strength requirements of single cold-formed channels connected back-to-back. *Journal of Constructional Steel Research* 62: 250-261.

Dundu, M. and Kemp, A. R. (2006b) Plastic and flexural behaviour of single cold-formed channels connected back-to-back. *Journal of Structural Engineering, ASCE,* 132(8), pp. 1223-1233.

Dundu M. 2003. The use of cold-rolled channels in light, small-span portal frames using back-to-back bolted connections in bearing. *Ph.D. thesis, School of Civil and Environmental Engineering, University of the Witwatersrand.*

ISO 6892-1. 2009. Metallic materials - Tensile testing. Part 1: Method of test at room temperature. Switzerland: *International Organisation for Standardization.*

SANS 10162-1. 2011. South Africa standard code of practice for the structural use of steel, Part 1 – Limit states design of hot-rolled steelwork. Pretoria: *SANS*.

SANS 10162-2. 2005. South Africa standard code of practice for the structural use of steel, Part 2 – Limit states design of cold-formed steelwork. Pretoria: *SANS*.